Quantum transport in porous media: Inelastic scattering of ^{4}He atoms and its temperature dependence

Zhao-Qing Zhang* and Ping Sheng†
Exxon Research & Engineering Company, Route 22 East, Annandale, New Jersey 08801
(Received 14 June 1993)

In porous media characterized by pore sizes in the range 5–20 Å, fluid transport characteristics at low temperatures may deviate significantly from the classical behavior, due to the interference effect arising from the quantum wave nature of the fluid atoms. An important consideration in this regard is the size and temperature dependence of the inelastic scattering length l_{in} for the fluid atom, which directly governs the magnitude of the quantum deviation. For a sample of size smaller than l_{in} the transport of the fluid atoms should be described by the Schrödinger equation confined in the pores. We intend to address this problem in two separate papers. In this paper we present the results of calculations for the inelastic scattering length in the case of a ^{4}He atom confined in a cylindrical pore. Inside the pore, a monolayer of physisorbed ^{4}He atoms is assumed to line the pore wall. Outside the pore, the solid material is assumed to be elastic. The thermal excitation of elastic waves results in the distortion of the cylindrical pore surface, which in turn causes transitions between the quantum eigenstates of ^{4}He inside the pore. By choosing some reasonable parameters of a porous medium, we have obtained the inelastic scattering rate (length) as a function of temperature for two pore radii. Our results show that the inelastic scattering length is on the order of 1 μm even at 50 K. This suggests that the quantum interference effect could be important at low temperatures, and that a deviation from Knudsen flow may be expected. The explicit calculation of quantum transport in this regime is planned to be the subject of a second paper.

PACS number(s): 47.55.Mh, 47.90.+a, 71.55.Jv

I. INTRODUCTION

Classical transport of gas or vapor in porous media is governed by the law of Knudsen flow [1]. Here, the mean-free path l of the particle is limited by the pore size, and the overall transport behavior is diffusive. The permeability κ, which is the ratio of flow rate to the pressure gradient, is given by $lv/3RT$. Since the mean velocity v is proportional to the square root of the temperature T, we have $\kappa \propto 1/\sqrt{T}$ as a characteristic of the Knudsen flow [2]. However, in the case where the particle is light and the pore radius is small enough so that the mean-free path l is comparable to the thermal wavelength λ, the quantum interference effect can become important and the classical treatment of diffusion is questionable. For instance, the value of λ for ^{4}He atoms at 10 K is about 2 Å. If the pore size is on the order of 10 Å, one would expect the flow behavior to deviate significantly from that described by the Knudsen flow. In addition, due to the coherent backscattering of the quantum-mechanical wave, one may also expect the reduction of permeability due to the localization effect [3]. However, the importance and observability of the quantum deviation depend crucially on the size of the inelastic scattering length being sufficiently large so that the coherent wave interference effect may have room to be established. There are at least two questions one can raise here. The first one is: What is the magnitude and dependence of the inelastic scattering length $l_{in}(T)$? The second one is: How are the permeability κ and its temperature dependence affected by $l_{in}(T)$? Intuitively, it is expected that $l_{in}(T)$ is a monotonically decreasing function of T because of the increasing number of modes participating in the inelastic scattering as T increases. The knowledge of $l_{in}(T)$ is of crucial importance in understanding and predicting the behavior of $\kappa(T)$. This is because experiments are always done on samples of finite size L. At low temperatures, when L is smaller than l_{in}, $\kappa(T)$ is governed by quantum diffusion, while at high temperatures a crossover to the Knudsen flow is anticipated when L becomes larger than l_{in}. We shall address these two questions in two separate papers.

In this first paper, we address only the first question, i.e., that concerning $l_{in}(T)$. For simplicity, we study the inelastic scattering rate of a single ^{4}He atom in an infinite cylindrical pore with a monolayer of ^{4}He atom physisorbed on its wall. The physisorption is attributed to the strong ^{4}He-wall attractive interaction [4,5]. The eigenstates of the single ^{4}He atom inside the pore is determined by its interaction with the ^{4}He-monolayer [6]. Below we give a schematic of the steps involved in the calculation of $l_{in}(T)$.

At finite temperatures, the thermal excitation of elastic waves in the medium surrounding the cylindrical hole is responsible for disturbing the wall boundary and for producing an interaction between the ^{4}He atom inside the wall and the excited elastic waves surrounding the wall. The first step in the calculation is therefore the deter-

*Present address: Dept. of Physics, Hong Kong University of Science and Technology, Clean Water Bay, Kowloon, Hong Kong.
†Also at Dept. of Physics, Hong Kong University of Science and Technology, Clean Water Bay, Kowloon, Hong Kong.

mination of the eigenstates and the eigenfrequencies of the elastic system. Through second quantization of the elastic eigenstates, the Born approximation is used to determine the transition probability of the ^{4}He atom as a function of temperature due to its coupling to the elastic excitations through the wall distortions. By choosing some reasonable parameters of a porous medium, the inelastic scattering time and length are then calculated for two different pore radii for temperatures ranging from 5 to 50 K. The results obtained show that, in contrast to the case of electrons in dirty metals, the inelastic scattering length of ^{4}He in a narrow cylindrical pore could be on the order of micrometers even at 50 K. This suggests that the quantum interference effect could play a dominant role in determining the permeability of dilute ^{4}He gas in narrow-channel porous media at low temperatures. Explicit calculation of the permeability is under way, and the results will be reported in a second paper. In what follows, Sec. II describes the formulation of the interaction Hamiltonian between a ^{4}He atom and the elastic waves surrounding the pore. Section III is devoted to the solution of various elastic eigenfunctions in a cylindrical geometry. Expressions for the inelastic scattering rate and numerical results are presented in Sec. IV. The paper concludes with a brief summary and discussion in Sec. V.

II. FORMULATIONS OF THE INTERACTION HAMILTONIAN

The inelastic scattering mechanism between the ^{4}He gas and a porous medium is simplified by considering the motion of a single ^{4}He atom in an infinite cylindrical pore surrounded by a homogeneous effective medium. Due to the strong attractive van der Waals interaction energy between the pore wall and the ^{4}He atom, on the order of 100 K [4,5] (in units of the Boltzmann constant k_B, same below), the first atoms passing through the channel are expected to be physisorbed and form a layer lining the wall. Once the layer is formed, the extra ^{4}He atom moving in the pore will interact only with the physisorbed ^{4}He atoms. To derive the interaction between the ^{4}He atom and the pore wall, we will further simplify the problem by assuming that (i) only one completely filled monolayer of ^{4}He is absorbed on the wall, i.e., neglecting all other possible fluctuations like partial coverage or the formation of multilayers; (ii) the monolayer is strongly bound to the wall, i.e., possessing no internal degree of freedom; (iii) the ^{4}He-pore surface interaction is completely shielded by the monolayer, and the extra atom will interact only with the monolayer; and (iv) the ^{4}He gas is so dilute that one can ignore the interaction among the ^{4}He atoms passing through the channel. The fourth assumption reduces the problem to a single-particle Hamiltonian, and Boltzmann statistics becomes applicable. By using the Lennard-Jones 6-12 potential for ^{4}He-^{4}He interaction [6],

$$V_{\rm LJ}(r)=4\varepsilon\left[\left[\frac{\sigma}{r}\right]^{12}-\left[\frac{\sigma}{r}\right]^{6}\right], \tag{1}$$

with $\varepsilon=10.22$ K, $\sigma=2.556$ Å and r the distance between two atoms, the total interaction potential between a single ^{4}He atom and the monolayer is of the form

$$V_T(\mathbf{r}')=4\varepsilon\sum_i\left[\left[\frac{\sigma}{|\mathbf{r}-\mathbf{r}_i|}\right]^{12}-\left[\frac{\sigma}{|\mathbf{r}'-\mathbf{r}_i|}\right]^{6}\right], \tag{2}$$

where $\mathbf{r}'$ and $\mathbf{r}_1$ are, respectively, the coordinates of the single atom and atoms in the monolayer. If we assume that the wall is smooth, the average distance between two nearest-neighbor atoms in the monolayer can be approximated by the values of r_0 which minimizes $V_{\rm LJ}(\mathbf{r})$. From $dV_{\rm LJ}(r)/dr=0$, we get $r_0=6\sqrt{2}\sigma\simeq 2.87$ Å. The centers of the monolayer atoms thus form a surface which in cylindrical coordinates can be represented by

$$\rho=a+\delta f(\phi,z), \tag{3}$$

where a is the radial distance from the center of the cylinder to the monolayer, and δf represents the perturbation of the wall surface caused by the elastic wave excitation surrounding the wall. Here cylindrical coordinates are used to represent δf.

The actual radius of the channel is the value a plus the distance between the monolayer and the wall, on the order of 3 Å. The explicit form of the function δf will be discussed in the next section. With the above description of the monolayer, we can approximate the summation in Eq. (2) by an integral that has the form

$$V_T(\rho',\phi',z')=\frac{4\varepsilon a}{r_0^2}\int_{-\infty}^{\infty}dz\int_0^{2\pi}d\phi[A^6-A^3], \tag{4}$$

with

$$A=\frac{\sigma^2}{(a+\delta f)^2+\rho'^2-2(a+\delta f)\rho'\cos(\phi-\phi')+(z-z')^2}. \tag{5}$$

Expanding A to the first order in δf, we find

$$V_T=V_T^0+\delta V_T, \tag{6}$$

where V_T^0 is the potential that affects the ^{4}He atom when the wall is rigid, i.e., $\delta f=0$ in Eq. (5), and δV_T has the form

$$\delta V_T(\rho',\phi',z')=\frac{4\varepsilon a}{r_0^2}\int_{-\infty}^{\infty}dz\int_0^{2\pi}d\phi[6A_0^5-3A_0^2]B\delta f(\phi,z), \tag{7}$$

with

$$B=\frac{2\sigma^2[\rho'\cos(\phi-\phi')-a]}{[a^2+\rho'^2-2a\rho'\cos(\phi-\phi')+(z-z')^2]^2}, \tag{8}$$

and A_0 is the expression given by Eq. (5) with $\delta f=0$. The interaction energy of the ^{4}He atom with the wall distortion can be written as

$$V_{\rm int}=\langle\psi|\delta V_T|\psi\rangle=\int d\mathbf{r}\,\psi^*(\mathbf{r})\delta V_T(\mathbf{r})\psi(\mathbf{r}), \tag{9}$$

where the wave function ψ of the ^{4}He atom can be expanded in terms of the eigenstates of unperturbed Hamiltonian, i.e.,

$$H_0\psi^0=\left[-\frac{\hbar^2}{2m_{\rm He}}\nabla^2+V_T^0\right]\psi^0=E^0\psi^0, \tag{10}$$

where m_{He} denotes the mass of a ^{4}He atom. For the convenience of numerical calculation, we assume here that the cylindrical hole is of finite length L, extending from $z=-L/2$ to $L/2$ with the periodical boundary condition at the two ends. Since V_T^0 depends only on ρ, we can write eigenfunctions in the form

$$\psi^0_{n,m,k}=R_{n,m}(\rho)\frac{e^{im\phi+ikz}}{\sqrt{2\pi L}} , \tag{11}$$

where m and k $(=2\pi q/L)$ are, respectively, the angular momentum quantum number and the wave vector along the z axis. Here m, n, and q denote integers, with n being the radial quantum number.

Substituting Eq. (11) into Eq. (10), we have

$$\left\{\frac{-\hbar^2}{2m_{\mathrm{He}}}\left[\frac{1}{\rho}\frac{\partial}{\partial\rho}\left[\rho\frac{\partial}{\partial\rho}\right]-\frac{m^2}{\rho^2}\right]+V_T^0(\rho)\right\}R_{n,m}(\rho)$$
$$=\left[E^0_{n,m,k}-\frac{\hbar^2k^2}{2m_{\mathrm{He}}}\right]R_{n,m}(\rho)\equiv E^0_{n,m}R_{n,m}(\rho) , \tag{12}$$

where $E^0_{n,m,k}$ is the eigenenergy of $\psi^0_{n,m,k}$. Numerical evaluation of $V_T^0(\rho)$ and the solutions to Eq. (12) will be given in Sec. IV. Once the function $\psi^0_{n,m,k}$ is known, the interaction energy can be written in a second quantized form by replacing $\psi(\mathbf{r})$ in Eq. (9) by a field operator

$$\psi(\mathbf{r})\equiv\sum_{n,m,k}\psi^0_{n,m,k}(\mathbf{r})a_{n,m,k} , \tag{13}$$

where $a_{n,m,k}$ is the annihilation operator of a ^{4}He atom in the state (n,m,k). This formulation will prove to be convenient in the later calculation. However, for explicit calculation the information about δf is required. This is the subject of the next section.

III. ELASTIC WAVE MODES IN THE CYLINDRICAL PORE GEOMETRY

In this section, we derive the elastic wave equation in the cylindrical pore geometry. The stress-free boundary condition at the pore wall is used to obtain the elastic wave excitations. Using these solutions, we second quantize the Hamiltonian for the elastic waves as well as δf. The inelastic scattering rate is then evaluated by using the Born approximation.

For simplicity, the porous medium and the ^{4}He monolayer adsorbed on the wall are considered as an effective medium in which there is a cylindrical pore with effective radius a. Let $(u_\rho(\mathbf{r}),u_\phi(\mathbf{r}),u_z(\mathbf{r}))$ be the displacement vector of the effective medium in cylindrical coordinates. The strain components in cylindrical coordinates can be derived [7] from the rectangular coordinates x_1,x_2,x_3 through a unitary transformation; i.e., from

$$\epsilon_{ij}=\tfrac{1}{2}\left[\frac{\partial u_j}{\partial x_i}+\frac{\partial u_i}{\partial x_j}\right] , \quad i,j=1,2,3 , \tag{14}$$

one obtains

$$\epsilon_{\rho\rho}=\frac{\partial u_\rho}{\partial\rho} , \tag{15a}$$

$$\epsilon_{\phi\phi}=\frac{u_\rho}{\rho}+\frac{\partial u_\phi}{\rho\partial\phi} , \tag{15b}$$

$$\epsilon_{zz}=\frac{\partial u_z}{\partial z} , \tag{15c}$$

$$\epsilon_{\rho\phi}=\epsilon_{\phi\rho}=\frac{1}{\rho}\frac{\partial u_\rho}{\partial\phi}-\frac{u_\phi}{\rho}+\frac{\partial u_\phi}{\partial\rho} , \tag{15d}$$

$$\epsilon_{z\phi}=\epsilon_{\phi z}=\frac{1}{\rho}\frac{\partial u_z}{\partial\phi}+\frac{\partial u_\phi}{\partial z} , \tag{15e}$$

$$\epsilon_{z\rho}=\epsilon_{\rho z}=\frac{\partial u_z}{\partial\rho}+\frac{\partial u_\rho}{\partial z} . \tag{15f}$$

The stress-strain relation remains in exactly the same form as for the rectangular coordinates [7]:

$$P_{\rho\rho}=(\lambda+2\mu)\epsilon_{\rho\rho}+\lambda\epsilon\phi\phi+\lambda\epsilon_{zz} , \tag{16a}$$

$$P_{\phi\phi}=\lambda\epsilon_{\rho\rho}+(\lambda+2\mu)\epsilon\phi\phi+\lambda\epsilon_{zz} , \tag{16b}$$

$$P_{zz}=\lambda\epsilon_{\rho\rho}+\lambda\epsilon\phi\phi+(\lambda+2\mu)\epsilon_{zz} , \tag{16c}$$

$$P_{\rho z}=\mu\epsilon_{\rho z} , \tag{16d}$$

$$P_{z\phi}=\epsilon_{z\phi} , \tag{16e}$$

$$P_{\rho\phi}=\mu\epsilon_{\rho\phi} . \tag{16f}$$

Here λ and μ are the Lamé coefficients of the effective medium. The determination of λ and μ from the material components will be described in the next section. The equation of motion in cylindrical coordinates can be written in the following component form:

$$\rho_0\frac{\partial^2u_\rho}{\partial t^2}=\frac{\partial P_{\rho\rho}}{\partial\rho}+\frac{\partial P_{\phi\rho}}{\rho\partial\phi}+\frac{\partial P_{z\rho}}{\partial z}+\frac{1}{\rho}(P_{\rho\rho}-P_{\phi\phi}) , \tag{17a}$$

$$\rho_0\frac{\partial^2u_\phi}{\partial t^2}=\frac{\partial P_{\rho\phi}}{\partial\rho}+\frac{\partial P_{\phi\phi}}{\rho\partial\phi}+\frac{\partial P_{z\phi}}{\partial z}+2\frac{P_{\phi\rho}}{\rho} , \tag{17b}$$

$$\rho_0\frac{\partial^2u_z}{\partial t^2}=\frac{\partial P_{\rho z}}{\partial\rho}+\frac{\partial P_{\phi z}}{\rho\partial\phi}+\frac{\partial P_{zz}}{\partial z}+\frac{P_{\rho z}}{\rho} , \tag{17c}$$

where ρ_0 is the mass-density of the effective medium. Substituting Eqs. (15) and (16) into (17), one obtains

$$\rho_0\frac{\partial^2u_\rho}{\partial t^2}=(\lambda+2\mu)\left[\frac{\partial^2u_\rho}{\partial\rho^2}+\frac{1}{\rho}\frac{\partial u_\rho}{\partial\rho}-\frac{u_\rho}{\rho^2}\right]$$
$$+\frac{(\mu+\lambda)}{\rho}\frac{\partial^2u_\rho}{\partial\phi\partial\rho}+(\lambda+\mu)\frac{\partial^2u_z}{\partial\rho\partial z}$$
$$+\frac{\mu}{\rho^2}\frac{\partial^2u_\rho}{\partial\phi^2}+\mu\frac{\partial^2u_\rho}{\partial z^2}-\frac{(\lambda+3\mu)}{\rho^2}\frac{\partial u_\phi}{\partial\phi} , \tag{18a}$$

$$\rho_0\frac{\partial^2u_\phi}{\partial t^2}=\frac{(\mu+\lambda)}{\rho}\left[\frac{\partial^2u_\rho}{\partial\phi\partial\rho}+\frac{\partial^2u_z}{\partial z\partial\phi}\right]$$
$$+\mu\left[\frac{\partial^2u_\phi}{\partial\rho^2}+\frac{\partial^2u_\phi}{\partial z^2}+\frac{1}{\rho}\frac{\partial u_\phi}{\partial\rho}-\frac{u_\phi}{\rho^2}\right]$$
$$+\frac{(\lambda+2\mu)}{\rho^2}\frac{\partial^2u_\phi}{\partial\phi^2}+\frac{(\lambda+3\mu)}{\rho^2}\frac{\partial u_\rho}{\partial\phi} , \tag{18b}$$

and

$$\rho_0\frac{\partial^2 u_z}{\partial t^2}=(\mu+\lambda)\left[\frac{\partial^2 u_\rho}{\partial\rho\partial z}+\frac{1}{\rho}\frac{\partial u_\rho}{\partial z}+\frac{\partial^2 u_\phi}{\rho\partial\phi\partial z}\right]+\mu\left[\frac{\partial^2 u_z}{\partial\rho^2}+\frac{\partial^2 u_z}{\rho^2\partial\phi^2}+\frac{1}{\rho}\frac{\partial u_z}{\partial\rho}\right]+(\lambda+2\mu)\frac{\partial^2 u_z}{\partial z^2}\ . \tag{18c}$$

These equations can be simplified by expressing them in terms of the potentials of $\mathbf{u}$, i.e.,

$$\mathbf{u}=\nabla\Phi+\nabla\times\mathbf{A}\ . \tag{19}$$

The scalar potential gives the longitudinal wave while the vector potential $\mathbf{A}$ gives the two transverse waves. Without losing generality, $\mathbf{A}$ can be written in terms of two scalar potentials γ and χ. In cylindrical coordinates, $\mathbf{A}$ has the form [8]

$$\mathbf{A}=\left[\frac{1}{\rho}\frac{\partial\gamma}{\partial\phi},\frac{-\partial\gamma}{\partial\rho},\chi\right]\ . \tag{20}$$

Substituting Eq. (20) into (19), we find

$$u_\rho=\frac{\partial\Phi}{\partial\rho}+\frac{1}{\rho}\frac{\partial\chi}{\partial\phi}+\frac{\partial^2\gamma}{\partial z\partial\rho}\ , \tag{21a}$$

$$u_\phi=\frac{1}{\rho}\frac{\partial\Phi}{\partial\phi}+\frac{1}{\rho}\frac{\partial^2\gamma}{\partial z\partial\phi}-\frac{\partial\chi}{\partial\rho}\ , \tag{21b}$$

$$u_z=\frac{\partial\Phi}{\partial z}-\frac{\partial^2\gamma}{\partial\rho^2}-\frac{1}{\rho}\frac{\partial\gamma}{\partial\rho}-\frac{1}{\rho^2}\frac{\partial^2\gamma}{\partial\phi^2}\ . \tag{21c}$$

In terms of the three scalar potentials, the new equations of motion are obtained by substituting Eq. (21) into Eq. (18). With some manipulation, we get

$$\frac{1}{\alpha^2}\frac{\partial^2\Phi}{\partial t^2}=\nabla^2\Phi=\frac{\partial^2\Phi}{\partial\rho^2}+\frac{1}{\rho}\frac{\partial\Phi}{\partial\rho}+\frac{\partial^2\Phi}{\rho^2\partial\phi^2}+\frac{\partial^2\Phi}{\partial z^2}\ , \tag{22a}$$

$$\frac{1}{\beta^2}\frac{\partial^2\gamma}{\partial t^2}=\nabla^2\gamma\ , \tag{22b}$$

$$\frac{1}{\beta^2}\frac{\partial^2\chi}{\partial t^2}=\nabla^2\chi\ , \tag{22c}$$

with

$$\alpha^2=(\lambda+2\mu)/\rho_0\ , \tag{22d}$$

$$\beta^2=\mu/\rho_0\ . \tag{22e}$$

Here α and β are, respectively, the sound velocities for the longitudinal and the transverse waves. Since the eigenmodes of Eq. (22) with the physical boundary condition have to be obtained numerically, we assume that the effective medium extends from $z=-L/2$ to $L/2$ and $\rho=a$ to b. Here b is the cutoff radius imposed for the convenience of numerical calculation. The stress-free boundary condition is applied on both the inner boundary $\rho=a$ and the outer boundary $\rho=b$. Similar to the case of the ^{4}He wave function in Eq. (11), the eigenfunction of Eq. (22) with frequency ω is of the form

$$F^{(i)}=\frac{R^{(i)}}{\sqrt{L}}\exp(im\phi)\exp(ikz)\exp(-i\omega t)\ , \tag{23}$$

where (i) stands for Φ, γ, and χ. Substituting Eq. (23) into Eq. (22), we find

$$\frac{\partial^2 R^{(\Phi)}}{\partial\rho^2}+\frac{1}{\rho}\frac{\partial R^{(\Phi)}}{\partial\rho}+\left[\frac{\omega^2}{\alpha^2}-k^2-\frac{m^2}{\rho^2}\right]R^{(\Phi)}=0\ , \tag{24a}$$

and

$$\frac{\partial^2 R^{(\gamma,\chi)}}{\partial\rho^2}+\frac{1}{\rho}\frac{\partial R^{(\gamma,\chi)}}{\partial\rho}+\left[\frac{\omega^2}{\beta^2}-k^2-\frac{m^2}{\rho^2}\right]R^{(\gamma,\chi)}=0\ . \tag{24b}$$

There are three different kinds of elastic waves, depending on the magnitude of ω^2 and k^2. If both $\omega^2/\alpha^2-k^2>0$ and $\omega^2/\beta^2-k^2>0$, then the solutions of Eq. (24) have the forms

$$R^{(\Phi)}=A_J^{(\Phi)}J_m(\bar{M}\rho)+A_N^{(\Phi)}N_m(\bar{M}\rho)\ , \tag{25a}$$

and

$$R^{(\gamma,\chi)}=A_j^{(\gamma,\chi)}J_m(\bar{Q}\rho)+A_N^{(\gamma,\chi)}N_m(\bar{Q}\rho)\ , \tag{25b}$$

with

$$\bar{M}=\left[\frac{\omega^2}{\alpha^2}-k^2\right]^{1/2};\qquad \bar{Q}=\left[\frac{\omega^2}{\beta^2}-k^2\right]^{1/2}, \tag{25c}$$

where J_m and N_m are Bessel functions of the first and second kinds and depend only on the absolute value of m [9]. The values of $A_J^{(i)}$ and $A_N^{(i)}$ are determined by the boundary condition, to be described later. When both $(\omega^2/\alpha^2)-k^2<0$ and $(\omega^2/\beta^2)-k^2<0$, the solutions of Eq. (24) become

$$R^{(\Phi)}=A_K^{(\Phi)}K_m(M\rho)+A_I^{(\Phi)}I_m(M\rho)\ , \tag{26a}$$

and

$$R^{(\gamma,\chi)}=A_K^{(\gamma,\chi)}K_m(Q\rho)+A_I^{(\gamma,\chi)}I_m(Q\rho)\ , \tag{26b}$$

with

$$M=\left[k^2-\frac{\omega^2}{\alpha^2}\right]^{1/2},\quad Q=\left[k^2-\frac{\omega^2}{\beta^2}\right]^{1/2},$$

where I_m and K_m are modified Bessel functions and depend only on the absolute value of m [9]. Thus, they represent localized surface modes decaying away from the boundaries $\rho=a$ or $\rho=b$. The third type of mode is the mixed type. Since $\alpha^2>\beta^2$ [see Eq. (22d)], we can have $\omega^2/\alpha^2-k^2<0$ but $\omega^2/\beta^2-k^2>0$. The solutions are in the form

$$R^{(\Phi)}=A_I^{(\Phi)}I_m(M\rho)+A_K^{(\phi)}K_m(M\rho)\ , \tag{27a}$$

$$R^{(\gamma,\chi)}=A_J^{(\gamma,\chi)}J_m(\bar{Q}\rho)+A_N^{(\gamma,\chi)}N_m(\bar{Q}\rho)\ , \tag{27b}$$

with

$$M=\left[k^2-\frac{\omega^2}{\alpha^2}\right]^{1/2},\quad \bar{Q}=\left[\frac{\omega^2}{\beta^2}-k^2\right]^{1/2}.$$

Equation (27) represents a surface mode for the longitudinal component and a propagating mode for the transverse components. To find the coefficient A's in the above solutions, we use stress-free boundary conditions on both the inner and the outer boundaries, i.e.,

$$P_{\rho\rho}(\rho=a,b)=P_{\rho\phi}(\rho=a,b)=P_{\rho z}(\rho=a,b)=0 \ . \quad (28)$$

From Eqs. (15), (16), and (21), Eq. (28) may be rewritten as

$$P_{\rho\rho}(\rho=a,b)=\left[-\rho_0\omega^2\Phi-2\mu\left[\frac{1}{\rho}\frac{\partial\Phi}{\partial\rho}+\frac{1}{\rho^2}\frac{\partial^2\Phi}{\partial\phi^2}+\frac{\partial^2\Phi}{\partial z^2}-\frac{\partial^2\chi}{\rho\partial\rho\partial\phi}+\frac{1}{\rho^2}\frac{\partial\chi}{\partial\phi}-\frac{\partial^3\gamma}{\partial z\partial\rho^2}\right]\right]_{\rho=a,b}=0 \ , \quad (29a)$$

$$P_{\rho\phi}(\rho=a,b)=\left[\frac{2}{\rho}\frac{\partial^2\Phi}{\partial\rho\partial\phi}+\frac{2}{\rho}\frac{\partial^3\gamma}{\partial\rho\partial\phi\partial z}-\frac{2}{\rho^2}\frac{\partial\Phi}{\partial\phi}-\frac{2}{\rho^2}\frac{\partial^2\gamma}{\partial\phi\partial z}+\frac{1}{\rho^2}\frac{\partial^2\chi}{\partial\phi^2}+\frac{1}{\rho}\frac{\partial\chi}{\partial\rho}-\frac{\partial^2\chi}{\partial\rho^2}\right]_{\rho=a,b}=0 \ , \quad (29b)$$

and

$$P_{\rho z}(\rho=a,b)=\rho_0\omega^2\frac{\partial\gamma}{\partial\rho}+2\mu\left[\frac{\partial^2\Phi}{\partial\rho\partial z}+\frac{\partial^3\gamma}{\partial\rho\partial z^2}+\frac{1}{\rho^3}\frac{\partial^2\gamma}{\partial\phi^2}+\frac{1}{\rho^3}\frac{\partial^2\gamma}{\partial\phi^2}+\frac{1}{2\rho}\frac{\partial^2\chi}{\partial z\partial\phi}\right]_{\rho=a,b}=0 \ , \quad (29c)$$

where Eqs. (22a) and (22b) have been used in deriving Eqs. (29a) and (29c). The eigenfrequency ω is determined by the existence of nontrivial solutions of A's which satisfy the above boundary conditions. For instance, in the case of propagating modes, by substituting Eqs. (23) and (25) into Eq. (29a), we find at $\rho=a$,

$$y_{1\Phi J}A_J^{(\Phi)}+y_{1\Phi N}A_N^{(\Phi)}+y_{1\gamma J}A_J^{(\gamma)}+y_{1\gamma N}A_N^{(\gamma)}+y_{1\chi J}A_J^{(\chi)}+y_{1\chi N}A_N^{(\chi)}=0 \ , \quad (30)$$

with

$$y_{1\Phi J}=\left[k^2+\frac{2m^2}{a^2}-\bar{Q}^2\right]J_m(\bar{M}a)-\frac{2\bar{M}}{a}J'_m(\bar{M}a) \ ,$$

$$y_{1\Phi N}=\left[k^2+\frac{2m^2}{a^2}-\bar{Q}^2\right]N_m(\bar{M}a)-\frac{2\bar{M}}{a}N'_m(\bar{M}a) \ ,$$

$$y_{1\gamma J}=2ik\bar{Q}^2J''_m(\bar{Q}a), \quad y_{1\gamma N}=2ik\bar{Q}^2N''_m(\bar{Q}a) \ , \quad (31)$$

$$y_{1\chi J}=i\left[\frac{2m}{a}\right]\left[\bar{Q}J'_m(\bar{Q}a)-\frac{1}{a}J_m(\bar{Q}a)\right] \ ,$$

$$y_{1\chi N}=i\left[\frac{2m}{a}\right]\left[\bar{Q}N'_m(\bar{Q}a)-\frac{1}{a}N_m(\bar{Q}a)\right] \ ,$$

where

$$J'_m(\bar{M}a)=dJm(z)/dz|_{z=\bar{M}a} \ .$$

The same definitions are used for $N'_m(\bar{M}a)$, $J''_m(\bar{Q}a)$, and $N'_m(\bar{Q}a)$. Also, Eqs. (22d) and (25c) have been used in deriving the relations for $y_{1\gamma J}$ and $y_{1\gamma N}$. Similarly, from Eqs. (29b) and (29c), we find

$$y_{2\Phi J}A_J^{(\Phi)}+y_{2\Phi N}A_N^{(\Phi)}+y_{2\gamma J}A_J^{(\gamma)}+y_{2\gamma N}A_N^{(\gamma)}+y_{2\chi J}A_J^{(\chi)}+y_{2\chi N}A_N^{(\chi)}=0 \ , \quad (32)$$

with

$$y_{2\Phi J}=i\left[\frac{2m}{a}\right]\left[\bar{M}J'_m(\bar{M}a)-\frac{1}{a}J_m(\bar{M}a)\right] \ , \quad (33a)$$

$$y_{2\Phi J}=i\left[\frac{2m}{a}\right]\left[\bar{M}N'_m(\bar{M}a)-\frac{1}{a}N_m(\bar{M}a)\right] \ , \quad (33b)$$

$$y_{2\gamma J}=\left[\frac{-2mk}{a}\right]\left[\bar{Q}J'_m(\bar{Q}a)-\frac{1}{a}J_m(\bar{Q}a)\right] \ , \quad (33c)$$

$$y_{2\gamma N}=\left[\frac{-2mk}{a}\right]\left[\bar{Q}N'_m(\bar{Q}a)-\frac{1}{a}N_m(\bar{Q}a)\right] \ , \quad (33d)$$

$$y_{2\chi J}=\frac{-m^2}{a^2}J_m(\bar{Q}a)+\frac{\bar{Q}}{a}J'_m(\bar{Q}a)-\bar{Q}^2J''_m(\bar{Q}a) \ , \quad (33e)$$

$$y_{2\chi N}=\frac{-m^2}{a^2}N_m(\bar{Q}a)+\frac{\bar{Q}}{a}N'_m(\bar{Q}a)-\bar{Q}^2N''_m(\bar{Q}a) \ , \quad (33f)$$

and

$$y_{3\Phi J}A_J^{(\Phi)}+y_{3\Phi N}A_N^{(\phi)}+y_{3\gamma J}A_J^{(\gamma)}+y_{3\gamma N}A_N^{(\gamma)}+y_{3\chi J}A_J^{(\chi)}+y_{3\chi N}A_N^{(\chi)}=0 \ , \quad (34)$$

with

$$y_{3\Phi J}=2ik\bar{M}J'_m(\bar{M}a) \ , \quad (35a)$$

$$y_{3\Phi N}=2ik\bar{M}N'_m(\bar{M}a) \ , \quad (35b)$$

$$y_{3\gamma J}=(\bar{Q}^2-k^2)\bar{Q}J'_m(\bar{Q}a)-\frac{2m^2}{a^3}J_m(\bar{Q}a) \ , \quad (35c)$$

$$y_{3\gamma N}=(\bar{Q}^2-k^2)\bar{Q}N'_m(\bar{Q}a)-\frac{2m^2}{a^3}N_m(\bar{Q}a) \ , \quad (35d)$$

$$y_{3\chi J}=-\frac{mk}{a}J_m(\bar{Q}a) \ , \quad (35e)$$

$$y_{3\chi N}=-\frac{mk}{a}N_m(\bar{Q}a) \ . \quad (35f)$$

Equations at the boundary $\rho=b$ are simply obtained from Eqs. (30)–(34) by replacing a with b. Thus we have

$$y_{i\Phi J}A_J^{(\phi)}+y_{i\Phi N}A_N^{(\Phi)}+y_{i\gamma J}A_J^{(\gamma)}+y_{i\gamma N}A_N^{(\gamma)}+y_{i\chi J}A_J^{(\chi)}+y_{i\chi N}A_N^{(\chi)}=0 \ , \quad i=4,5, \text{ and } 6 \ , \quad (36)$$

where y_{4PQ}, y_{5PQ}, and y_{6PQ} are, respectively, the same expressions as y_{1PQ}, y_{2PQ}, and y_{3PQ} with a replaced by b. Here the index P stands for Φ, γ, and χ, and Q stands for J and N. We thus have six homogeneous equations with six unknowns A_Q^P. The nontrivial solutions are deter-

mined by the condition

$$\det[y_{ij}]=0 , \tag{37}$$

where $i=i,\ldots,6$ and j corresponds to the vector $[\Phi J,\Phi N,\gamma J,\gamma N,\chi J,\chi N]$. Thus $y_{14}=y_{1\gamma N}$, for examples. For given values of m and k, Eq. (37) is solved numerically for the roots $\{\omega_i\}$, which in turn give the nontrivial solutions of A_Q^P up to an arbitrary constant. Similarly, the same method applies to the case of surface modes and mixed modes. The corresponding equations are given in the Appendix. Knowing the eigensolutions for the scalar potential, the corresponding physical eigenstates, in terms of the displacement vector $\mathbf{u}=(u_\rho,u_\phi,u_z)$, can be obtained from Eq. (21). In fact, it is straightforward to show that with our physical boundary condition, expressed by Eqs. (28) and (29), the operator L on the right-hand side of Eq. (18) is Hermitian, i.e.,

$$\int_\Omega \mathbf{u}\cdot L(\mathbf{v})d\mathbf{r}=\int_\Omega \mathbf{v}\cdot L(\mathbf{u})d\mathbf{r} \tag{38}$$

for any two solutions $\mathbf{u},\mathbf{v}$ satisfying Eq. (29), and Ω is the volume occupied by the effective medium. Thus, the eigenfunctions $\mathbf{u}_\alpha$ are mutually orthogonal, and the arbitrary constant in A_Q^P may be determined by the normalization condition, i.e.,

$$\int_\Omega \mathbf{u}_\alpha^*\cdot\mathbf{u}_\beta d\mathbf{r}=\delta_{\alpha\beta} , \tag{39}$$

where α stands for an eigenstate with fixed m, k, and $\omega_i(m,k)$, with $\omega_i(m,k)$ denoting the ith eigenmode at given m and k. This completes the solution procedure for the eigenfrequencies and the eigenfunctions of the elastic wave excitations.

Next, we second quantize the elastic waves. The procedure is parallel to the quantization of elastic waves in rectangular coordinates [10]. First we notice that the Lagrangian corresponding to Eq. (18) can be written in the following form:

$$\mathcal{L}=\frac{\rho_0}{2}\int_\Omega \dot{\mathbf{u}}\cdot\dot{\mathbf{u}}\,d\mathbf{r}+\tfrac{1}{2}\int_\Omega \mathbf{u}\cdot L(\mathbf{u})d\mathbf{r} , \tag{40}$$

where the force equation (18) has been used to derive the potential-energy term. The Hamiltonian then has the form

$$H=\frac{1}{2\rho_0}\int_\Omega \mathbf{p}\cdot\mathbf{p}\,d\mathbf{r}-\tfrac{1}{2}\int_\Omega \mathbf{u}\cdot L(\mathbf{u})d\mathbf{r} , \tag{41}$$

where

$$\mathbf{p}=\frac{\delta\mathcal{L}}{\delta\dot{\mathbf{u}}}=\rho_0\dot{\mathbf{u}} \tag{42}$$

is the momentum density. In the second quantized form, the displaced field operator $\mathbf{U}$ and its conjugate momentum $\mathbf{P}$ take the forms

$$\mathbf{U}=\sum_\alpha\left[\frac{\hbar}{2\rho_0\omega_\alpha}\right]^{1/2}(\mathbf{u}_\alpha^*\xi_\alpha^\dagger+\mathbf{u}_\alpha\xi_\alpha) \tag{43}$$

and

$$\mathbf{P}=i\sum_\alpha\left[\frac{\hbar\rho_0\omega_\alpha}{2}\right]^{1/2}(\mathbf{u}_\alpha^*\xi_\alpha^\dagger-\mathbf{u}_\alpha\xi_\alpha) , \tag{44}$$

where α sums all eigenstates $\{m,k,\omega_\alpha(m,k)\}$ with the corresponding eigenfrequency $\omega_\alpha\equiv\omega_\alpha(m,k)$ and eigenfunction $\mathbf{u}_\alpha$. $\xi_\alpha^\dagger$ and ξ_α are, respectively, the boson creation and annihilation operators. It is easy to check that $\mathbf{U}$ and $\mathbf{P}$ have the following commutation relation:

$$[\mathbf{U},\mathbf{P}]=i\hbar\sum_\alpha 1 , \tag{45}$$

so the Hamiltonian of Eq. (41) becomes

$$H=\hbar\sum_\alpha\omega_\alpha(\xi_\alpha^\dagger\xi_\alpha+\tfrac{1}{2}) . \tag{46}$$

Now we are ready to write down the explicit form of surface perturbation δf required in the interaction energy expression of Eqs. (7)–(9). Since the components u_ϕ and u_z do not alter the shape of the wall surface, only u_ρ is relevant. We have

$$\delta f(\phi,z)=\sum_\alpha\left[\frac{\hbar}{2\rho_0\omega_\alpha}\right]^{1/2}\{[u_\rho^*(\rho=a)]_\alpha\xi_\alpha^\dagger+[u_\rho(\rho=a)]_\alpha\xi_\alpha\} . \tag{47}$$

Equation (47) completes our construction of $H_{\rm int}$ between a ^{4}He atom inside the pore and the elastic phonons in the effective medium. In the next section we derive the expression for the inelastic scattering rate and present results of numerical calculations.

IV. INELASTIC TRANSITION RATE AND ITS NUMERICAL EVALUATION

By combining Eqs. (7), (9), (13), and (47), with a change of coordinates in the integration of Eq. (7), the interaction Hamiltonian can be written in the following second quantized form:

$$H_{\rm int}=\sum_{n,n',m',k'm,k}\sum_{\omega_i(m,k)}\left[\frac{\hbar}{2\rho_0\omega_i L}\right]^{1/2}\int_0^a\rho'd\rho'\{R^*_{n,m'-m}(\rho')R_{n',m'}(\rho')\delta\bar{V}_{m,k}(\rho')[u_\rho^*(a)]_{m,k,\omega_i}\times a^\dagger_{n,m'-m,k'-k}a_{n',m',k'}\xi^\dagger_{m,k,\omega_i}+\text{H.c.}\} , \tag{48}$$

with

$$\delta\bar{V}_{m,k}(\rho')=\frac{4\epsilon a}{r_0^2}\int_{-L/2}^{L/2}dy\int_0^{2\pi}d\theta(6\bar{A}^5_0-3\bar{A}^2_0)\bar{B}e^{i(m\theta+ky)} , \tag{49}$$

where $\bar{A}_0$ and $\bar{B}$ have the same expressions as A_0 and B in Eqs. (5) and (8) but with $\phi-\phi'$ and $z-z'$ replaced by θ and y, respectively. $H_{\rm int}$ has the standard form of electron-phonon interaction. The first term in Eq. (48) represents the creation of an elastic phonon of quantum number $\{m,k,\omega_i(m,k)\}$. The total angular momentum and the momentum in the z direction are both conserved during the scattering process. The Hermitian conjugate (H.c.) term in Eq. (48) represents the annihilation process.

With the explicit form of $H_{\rm int}$, we can now calculate the transition rate by using the standard Born approximation [11]. To calculate the inelastic scattering rate, the fluid we are considering here is ^{4}He gas in the dilute limit so that the interaction between ^{4}He atoms can be ignored and condensation of ^{4}He atoms is suppressed to very low temperature, not in the range of our interest here. At finite temperature T, Boltzmann statistics are used for the states associated with the single ^{4}He atom, while Bose statistics are used for the elastic phonons. Following the standard procedure, the transition rate, or the inverse inelastic scattering time $\tau_{\rm in}$, is found to be

$$\frac{1}{\tau_{\rm in}}=\frac{\pi}{\rho_0 Z_{\rm He}}\sum_{n',m'k'} e^{-E_{n',m',k'}/k_BT}\sum_{n,m,k,\omega_i(m,k)}\left\{\frac{(n_{m,k,\omega_i}+1)}{\omega_i}|X^+_{n,n',m',m,k,\omega_i}|^2\delta(E^0_{n,m'-m,k'-k}-E^0_{n',m',k}+\omega_i\hbar)\right.$$
$$\left.+\frac{n_{m,k,\omega_i}}{\omega_i}|X^-_{n,n',m',m,k,\omega_i}|^2\delta(E^0_{n,m'+m,k'+k}-E^0_{n',m',k}-\omega_i\hbar)\right\}, \quad (50)$$

where

$$X^+_{n,n',m',m,k,\omega_i}=\int_0^a \rho\,d\rho\,R^*_{n,m'-m}(\rho)R_{n',m'}(\rho)\times\delta\bar{V}_{m,k}(\rho)[u^*_\rho(a)]_{m,k,\omega_i}, \quad (51)$$

and

$$X^-_{n,n',m',m,k,\omega_i}=\int_0^a \rho\,d\rho\,R^*_{n,m'+m}(\rho)R_{n',m'}(\rho)\times\delta\bar{V}_{m,k}(\rho)[u_\rho(a)]_{m,k,\omega_i}. \quad (52)$$

In Eq. (50), $Z_{\rm He}$ denotes the partition function of the ^{4}He atom. It has the form

$$Z_{\rm He}=\sum_{n',m',k'} e^{-E^0_{n',m',k'}/k_BT}. \quad (53)$$

Here $E^0_{n',m',k'}$ is the initial-state ^{4}He energy obtained from Eq. (12) (numerically), and n_α is the phonon occupation probability, i.e.,

$$n_\alpha=\frac{1}{\exp(\omega_\alpha/k_BT)-1}. \quad (54)$$

The terms containing $|X^+|^2$ and $|X^-|^2$ correspond to the phonon creation and annihilation processes, respectively, and the factors $(n_\alpha+1)$ and n_α are terms obtained from the phonon averages of $\langle\xi_\alpha\xi^\dagger_\alpha\rangle$ and $\langle\xi^\dagger_\alpha\xi_\alpha\rangle$, respectively [12]. Equation (50) forms the basis of our numerical calculations.

The numerical calculations are divided into three steps. In the first step, we solve Eq. (12) numerically for the eigenvalues $E^0_{n,m}$ and eigenfunctions $R_{n,m}(\rho)$ of a ^{4}He atom for various m. Since Eq. (12) depends only on m^2, we only will solve for $m\geq 0$. For states with nonzero k, the radial wave function $R_{n,m}(\rho)$ remains unchanged from that with $k=0$, but the energy becomes $E^0_{n,m,k}=E^0_{n,m}+\hbar^2k^2/2m_{\rm He}$. The function $V^0_T(\rho)$ can be integrated numerically by using Eq. (4). First we consider the case $a=7.5$ Å. The curve $V^0_T(\rho)$ is plotted in Fig. 1. Since we are interested in the value of $\tau_{\rm in}$ up to 50 K, the number of eigenstates we have to use for a fixed m is such that the highest excitation energy is always greater than 100 K. For instance, when $m=0$, the highest value of n we have solved is $n=7$, which has an energy $E^0_{7,0}=102.11$ K. Compared to the ground-state energy $E^0_{0,0}=-18.70$ K, and excitation energy is $\Delta E=102.11$ K$+18.70$ K$=120.81$ K, which is more than twice the maximum temperature, 50 K, we are interested in, so that the calculation should be accurate. As m increases, the number of n decreases for a fixed maximum energy. The highest m we have used is $m=19$. In this case only the state with $n=0$ is used so that $E^0_{0,19}=83.17$ K and excitation energy $\Delta E=101.87$ K. In Figs. 2 and 3, we plot some lower-energy states for the cases $m=0$ and 1, respectively. The total number of ^{4}He states used are 84.

The second step in our calculation is the solution of the elastic phonon problem described in Sec. III. Before solving Eq. (37) for the eigenmodes, we have to know the parameters ρ_0, λ, and μ of the effective medium. By using the porous silica as our model, the mass density of sil-

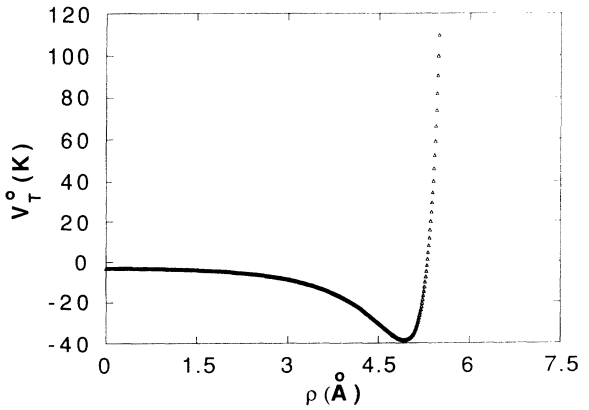

FIG. 1. Potential $V^0_T(\rho)$ acting upon a ^{4}He atom in a cylindrical pore with a lining of ^{4}He atoms. The effective pore radius is 7.5 Å, and ρ is the radial distance.

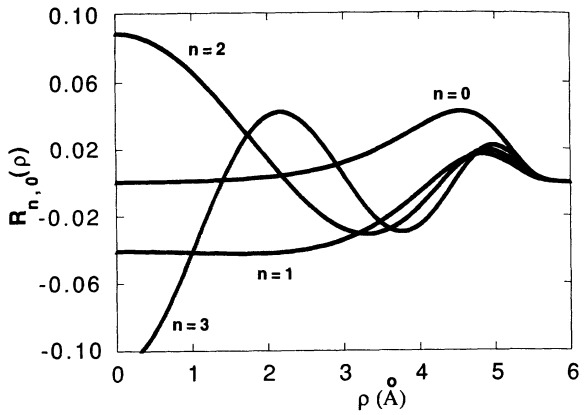

FIG. 2. Renormalized radial wave functions for $n=0,1,2,3$ with $m=0$ and a pore radius $a=7.5$ Å.

ica is 2.3 g/cm^3. Taking into account the porosity, we multiply it by a volume fraction of $p=0.75$ to obtain $\rho_0=1.725$ g/cm^3. The Lamé constants of crystalline silica are $\lambda_s=1.61\times10^{10}$ N/m^2 and $\mu_s=3.12\times10^{10}$ N/m^2. The effective parameters λ and μ can be obtained from the effective-medium theory [13]. By choosing $p=0.75$, we find $\lambda=0.881\times10^{10}$ N/m^2 and $\mu=1.548\times10^{10}$ N/m^2, respectively. The inner boundary has a radius $a=7.5$ Å, and the outer boundary is fixed at 750 Å. Since $b/a=100$, we believe this choice of b to be a good approximation to an infinite bulk system. The value of L is chosen to be $2\pi/0.001\cong6283$ Å. For each given m and k, $\{\omega_i(m,k)\}$ are obtained numerically from the roots of Eq. (37) for all three types of modes. We have cut off the solutions with energy $\hbar\omega_i$ greater than 100 K. Since the number of modes within 100 K decreases as k increases, the maximum value of k used is 0.4 Å^{-1}, above which there exists no mode with energy less than 100 K. Also, it is observed that as m increases, it causes more energy to sustain the same magnitude of u_ρ at $\rho=a$. In fact, the value of $u_\rho(a)$ decreases drastically as m increases for modes of similar energy. We have chosen the maximum m value to be $m_{\max}=4$. Further increase of $m_{\max}$ to 6 does not produce any significant change in $\tau_{\rm in}$. The total number of modes obtained is 402 882, of which 215 036 come from bulk modes, 187 713 come from mixed modes, and only 133 come from $m=0$ surface modes. Although the number of surface modes counter is rather small, its displacement $u_\rho(a)$ is at least two to three orders of magnitude greater than that of the other two kinds of modes, due to its localized surface mode nature. Thus, the contribution from the surface mode is important in the calculation of $\tau_{\rm in}$.

The third step in the calculation is the evaluation of Eq. (50). In fact, the δ function in Eq. (50) can be integrated directly, and this leads to a simpler expression. The result of inelastic scattering time is plotted as curve A of Fig. 4 on a log-log scale. The inelastic scattering length $l_{\rm in}$ is related to the inelastic scattering time $\tau_{\rm in}$ by the relation $l_{\rm in}\simeq\sqrt{D_0\tau_{\rm in}}$, when D_0 is the classical diffusion constant and has the value $D_0\simeq vl/3$, where v is the average velocity of a ^{4}He atom in the z direction. It is simple to show that the Boltzmann statistics give $v=\sqrt{k_BT/m_{\rm He}}$. As a lower bound estimate, we take the mean-free path as the effective channel diameter, i.e., $l\cong2a$. Thus, we have

$$l_{\rm in}\simeq\left[\frac{(k_BT)}{m_{\rm He}}\right]^{1/4}\left[\frac{2a\tau_{\rm in}}{3}\right]^{1/2}. \tag{55}$$

The numerical result on $l_{\rm in}$ is plotted in curve A of Fig. 5 from $T=5$ K to 50 K. We have also calculated $\tau_{\rm in}$ and $l_{\rm in}$ for the case of effective pore radius $a=15$ Å. The values of b and L remain unchanged here, i.e., $b=750$ Å and $L\cong6283$ Å. Using the same criterion, i.e., excitation energy less than 100° K as the cutoff, we have calculated 359 ^{4}He atom eigenstates, $E^0_{n,m}$ and $R_{n,m}(\rho)$, from Eq. (12), of which 17 states ($n=16$) belong to the case $m=0$. The maximum value of m calculated is 47. The total number of elastic waves calculated in this case is 402 148, of which 215 351 belong to the bulk mode, 186 608 belong to the mixed mode, and 189 are from the $m=0$ surface mode. The results of $\tau_{\rm in}$ and $l_{\rm in}$ are plotted as curves B of Figs. 4 and 5. It is expected that the larger the radius a, the shorter the inelastic scattering time. This is because a

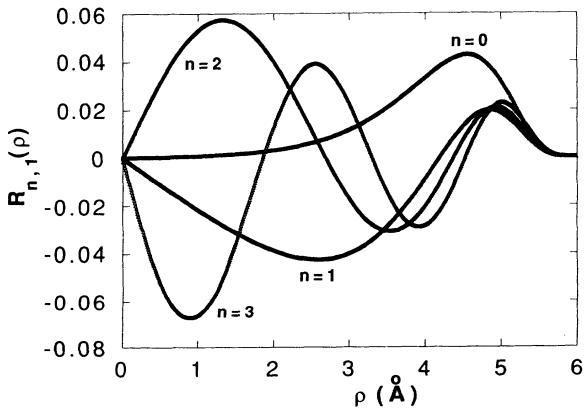

FIG. 3. Renormalized radial wave functions for $n=0,1,2,3$ with $m=1$ and a pore radius $a=7.5$ Å.

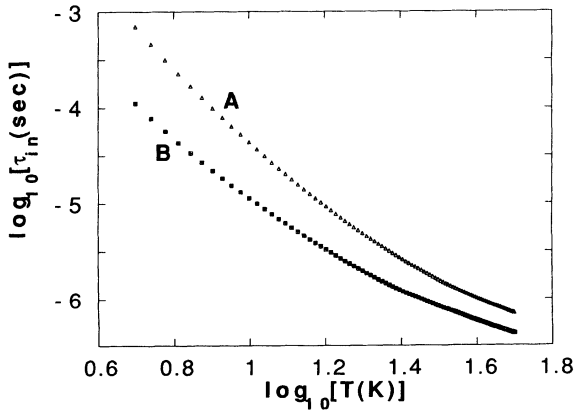

FIG. 4. Log-log plot of the inelastic scattering time $\tau_{\rm in}$ (sec) as a function of temperature ranging from 5–50 K, for the cases $a=7.5$ Å (curve A) and $a=15$ Å (curve B).

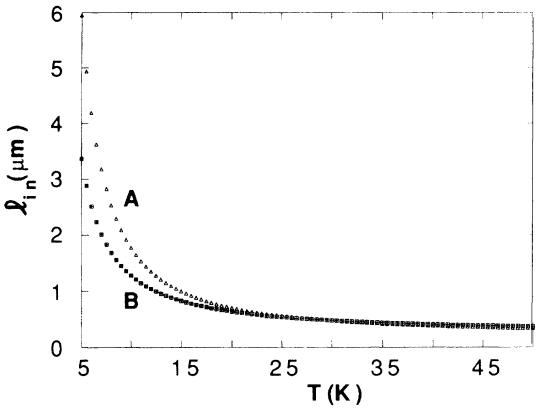

FIG. 5. Inelastic scattering length l_{in}, in units of micrometers, is plotted as a function of temperature ranging from 5−50 K. Curves A and B are, respectively, for the cases $a=7.5$ and 15 Å.

large radius reduces the level spacing between the ^{4}He states, $E^0_{n,m}$ and therefore increases the density of states and the transmission rate. However, this difference is compensated to some extent by the factor $\sqrt{a}$ [Eq. (55)] in the inelastic scattering length. This compensation effect is particularly apparent at the high-temperature region where the ratio between the values of τ_{in} for $a=7.5$ Å and 15 Å is about 2, but the values for l_{in} are about the same in the two cases. From Fig. 5 it is seen that in both cases, l_{in} decays slowly in the high temperature region, partly due to the $(T)^{1/4}$ factor in Eq. (55). Although the accuracy of our calculated results is expected to decrease as T increases, even in the worst case of $T\simeq 50$ K, our results are still believed to be correct to within 10–20 %.

We have tested the convergency of our calculation by using a system of size $b=75$ Å, $a=7.5$ Å, and $L=3142$ Å. For temperatures below 20 K we find less than a 5% increase in the inelastic scattering time from that of Fig. 4. The Lamé constants of the porous medium used in this work are about a factor of 2 larger than those of Vycor glass of porosity 28% and density 1.56 g/cm^2 [14]. The measured values of Vycor are $\lambda=0.49\times10^{10}$ N/m^2 and $\mu=0.75\times10^{10}$ N/m^2 [15], compared to $\lambda=0.881\times10^{10}$ N/m^2 and $\mu=1.548\times10^{10}$ N/m^2 used in this work. The effects of the smaller Lamé constants on the inelastic scattering time can be estimated in the following way. Smaller Lamé constants give smaller sound speeds that in turn increase the density of states of the elastic wave and reduce the inelastic scattering time. The effective medium Lamé constants and density used in this work give a longitudinal sound speed $\alpha=4801$ m/sec and a transverse sound speed $\beta=2996$ m/sec. These numbers are 35% larger than the corresponding measured values of Vycor samples of porosity 28%, which have $\alpha=3570$ m/sec and $\beta=2190$ m/sec. Since the density of states is inversely proportional to the sound speed, in Vycor there are 35% more modes contributing to the inelastic scattering process. Thus, the Lamé constants we used here may result in an inelastic scattering length which is 35% larger than that in Vycor. However, the qualitative conclusion of this work, i.e., l_{in} decays slowly in the high-temperature region and is on the order of micrometers even at 50 K, are not altered.

V. DISCUSSION

It should be pointed out that in our model we have assumed an ideal pore channel possessing both azimuthal symmetry and translational symmetry in the z direction. Therefore, during a scattering process, the selection rules require the conservation of both the angular momentum and the translational momentum in the z direction. However, in real porous media, the channels are always tortuous and nonuniform. The broken symmetry would allow transitions that are forbidden in the perfect symmetry case, thereby increasing the total number of inelastic scatterings. The scattering amplitude, though, will in general be reduced compared to that of allowed transitions in the symmetrical case. The combining effect is expected to change our results quantitatively, but not qualitatively. Also, the inelastic scattering length calculated here is noted to be measured along the pore channel. For a tortuous pore channel, the straight-line measure could be smaller due to the tortuosity. For these two reasons, the actual inelastic scattering length in porous media is expected to be smaller. Nevertheless, the important conclusion we can draw from our calculation is that at temperatures below 20 K, mesoscopic samples that are micrometer in size can exhibit strong quantum interference effect in the transport of ^{4}He gas in pores that are on the order of 10 Å. Strong deviation from Knudsen flow could be expected in this regime, and a new quantum-mechanical treatment of the transport property is thus required. The localization of ^{4}He is a strong possibility in these materials. It is suggested that if the localization effect is present, then the easiest way to observe that is through the temperature dependence of the permeability. The reasoning is as follows. Classically, Knudsen flow gives the temperature dependence of $\kappa(T)\sim 1/(T)^{-2}$, i.e., flow becomes easier as temperature decreases. However, if the quantum interference is present, then the weak localization effect (coherent backscattering) is known to be directly dependent on the size of l_{in}, i.e., localization effect increases as l_{in} increases. Since our calculation shows that l_{in} increases sharply at low temperatures, it is expected that it can lead to a lower transport coefficient, or even an opposite temperature dependence of $\kappa(T)$ from that predicted by the Knudsen flow. Any experimental verification of such behavior would be not only interesting but also important for the further understanding of quantum permeation. Explicit calculations of quantum transport in this regime is now underway. The results will be reported in a second paper.

ACKNOWLEDGMENTS

We wish to thank Minyao Zhou and B. Abeles for many helpful discussions.

APPENDIX

To obtain the boundary equations that determine the surface modes, we substitute Eqs. (23) and (26) into Eq. (29) and yield

$$y_{i\Phi K}A_K^{(\Phi)}+y_{i\Phi I}A_I^{(\Phi)}+y_{i\gamma K}A_K^{(\gamma)}+y_{i\gamma I}A_I^{(\gamma)}+y_{i\chi K}A_K^{(\chi)}+y_{i\chi I}A_I^{(\chi)}=0\ ,\quad i=1,2,\ldots,6 \tag{A1}$$

with

$$y_{1\Phi K}=\left[k^2+Q^2+\frac{2m^2}{a^2}\right]K_m(Ma)-\frac{2M}{a}K'_m(Ma)\ ,$$

$$y_{1\Phi I}=\left[k^2+Q^2+\frac{2m^2}{a^2}\right]I_m(Ma)-\frac{2M}{a}I'_m(Ma)\ ,$$

$$y_{1\gamma K}=2ikQ^2K''_m(Qa)\ ,$$

$$y_{1\gamma I}=2ikQ^2I''_m(Qa)\ ,$$

$$y_{1\chi K}=i\left[\frac{2m}{a}\right]\left[QK'_m(Qa)-\frac{1}{a}K_m(Qa)\right]\ ,$$

$$y_{1\chi I}=i\left[\frac{2m}{a}\right]\left[QI'_m(Qa)-\frac{1}{a}I_m(Qa)\right]\ , \tag{A2}$$

$$y_{2\Phi K}=i\left[\frac{2m}{a}\right]\left[MK'_m(Ma)-\frac{1}{a}K_m(Ma)\right]\ ,$$

$$y_{2\Phi I}=i\left[\frac{2m}{a}\right]\left[MI'_m(Ma)-\frac{1}{a}I_m(Ma)\right]\ ,$$

$$y_{2\gamma K}=\frac{2km}{a}\left[\frac{1}{a}K_m(Qa)-QK'_m(Qa)\right]\ ,$$

$$y_{2\gamma I}=\frac{2km}{a}\left[\frac{1}{a}I_m(Qa)-QI'_m(Qa)\right]\ ,$$

$$y_{2\chi K}=\frac{-m^2}{a^2}K_m(Qa)+\frac{Q}{a}K'_m(Qa)-Q^2K''_m(Qa)\ ,$$

$$y_{2\chi I}=\frac{-m^2}{a^2}I_m(Qa)+\frac{Q}{a}I'_m(Qa)-Q^2I''_m(Qa)\ ,$$

$$y_{3\Phi K}=2ikMK'_m(Ma)\ ,$$

$$y_{3\Phi I}=2ikMI'_m(Ma)\ ,$$

$$y_{3\gamma K}=-(k^2+Q^2)QK'_m(Qa)-\frac{2m^2}{a^3}K_m(Qa)\ ,$$

$$y_{3\gamma I}=-(k^2+Q^2)QI'_m(Qa)-\frac{2m^2}{a^3}I_m(Qa)\ ,$$

$$y_{3\chi K}=\frac{-km}{a}K_m(Qa)\ ,$$

$$y_{3\chi I}=\frac{-km}{a}I_m(Qa)\ ,$$

and

$$y_{4PQ}=y_{1PQ}(a\to b)\ ,$$

$$y_{5PQ}=y_{2PQ}(a\to b)\ ,$$

$$y_{6PQ}=y_{3PQ}(a\to b)\ ,$$

for $p=\Phi$, γ, and χ and $Q=K$ and I. Similarly for mixed modes, we have substituted Eqs. (23) and (27) by Eq. (29). The following equations are obtained:

$$y_{i\Phi K}A_K^{(\Phi)}+y_{i\Phi I}A_I^{(\Phi)}y_{i\gamma J}A_J^{(\gamma)}+y_{i\gamma N}A_N^{(\gamma)}+y_{i\chi J}A_J^{(\chi)}+y_{i\chi N}A_N^{(\chi)}=0\ ,\quad i=1,2,\ldots,6\ , \tag{A3}$$

with

$$y_{1\Phi K}=\left[k^2-\bar{Q}^2+\frac{2m^2}{a^2}\right]K_m(Ma)-\frac{2M}{a}K'_m(Ma)\ ,$$

$$y_{1\Phi I}=\left[k^2-\bar{Q}^2+\frac{2m^2}{a^2}\right]I_m(Ma)-\frac{2M}{a}I'_m(Ma)\ ,$$

$$y_{1\gamma J}=2ik\bar{Q}^2J''_m(\bar{Q}a)\ ,$$

$$y_{1\gamma N}=2ik\bar{Q}^2N''_m(\bar{Q}a)\ ,$$

$$y_{1\chi J}=i\left[\frac{2m}{a}\right]\left[\bar{Q}J'_m(\bar{Q}a)-\frac{1}{a}J_m(\bar{Q}a)\right]\ ,$$

$$y_{1\chi N}=i\left[\frac{2m}{a}\right]\left[\bar{Q}N'_m(\bar{Q}a)-\frac{1}{a}N_m(\bar{Q}a)\right]\ ,$$

$$y_{2\Phi K}=i\left[\frac{2m}{a}\right]\left[MK'_m(Ma)-\frac{1}{a}K_m(Ma)\right]\ ,$$

$$y_{2\Phi I}=i\left[\frac{2m}{a}\right]\left[MI'_m(Ma)-\frac{1}{a}I_m(Ma)\right]\ ,$$

$$y_{2\gamma J}=\frac{2km}{a}\left[\frac{J_m(\bar{Q}a)}{a}-\bar{Q}J'_m(\bar{Q}a)\right]\ ,$$

$$y_{2\gamma N}=\frac{2km}{a}\left[\frac{N_m(\bar{Q}a)}{a}-\bar{Q}N'_m(\bar{Q}a)\right]\ ,$$

$$y_{2\chi J}=\frac{-m^2}{a^2}J_m(\bar{Q}a)+\frac{\bar{Q}}{a}J'_m(\bar{Q}a)-\bar{Q}^2J''_m(\bar{Q}a)\ ,$$

$$y_{2\chi N}=\frac{-m^2}{a^2}N_m(\bar{Q}a)+\frac{\bar{Q}}{a}N'_m(\bar{Q}a)-\bar{Q}^2N''_m(\bar{Q}a)\ ,$$

$$y_{3\Phi K}=i2kMK'_m(Ma)\ ,$$

$$y_{3\Phi I}=i2kMI'_m(Ma)\ ,$$

$$y_{3\gamma J}=(\bar{Q}^2-k^2)\bar{Q}J'_m(\bar{Q}a)-\frac{2m^2}{a^3}J_m(\bar{Q}a)\ ,$$

$$y_{3\gamma N}=(\bar{Q}^2-k^2)\bar{Q}N'_m(\bar{Q}a)-\frac{2m^2}{a^3}N_m(\bar{Q}a)\ ,$$

$$y_{3\chi J}=-\frac{mk}{a}J_m(\bar{Q}a)\ ,$$

$$y_{3\chi N}=-\frac{mk}{a}N_m(\bar{Q}a)\ ,$$

and

$$y_{4PQ}=y_{1PQ}(a\to b)\ ,$$

$$y_{5PQ}=y_{2PQ}(a\to b)\ ,$$

$$y_{6PQ}=y_{3PQ}(a\to b)\ ,$$

for $(PQ)=(\Phi K)$, (ΦI), (γJ), (γN), (χJ), and (χN).

[1] M. Knudsen, Avin Physik **28**, 75 (1909).
[2] See, for example, B. Abeles, L. F. Chen, J. W. Johnson, and J. M. Drake, Isr. J. Chem. **31**, 99 (1991).
[3] See, for example, P. A. Lee and T. V. Ramakrishnan, Rev. Mod. Phys. **57**, 287 (1985).
[4] A. D. Novaco and C. E. Campbell, Phys. Rev. B **11**, 2525 (1975).
[5] R. H. Tait and J. D. Reppy, Phys. Rev. B **20**, 997 (1979).
[6] L. W. Brach and I. J. McGee, J. Chem. Phys. **46**, 2959 (1967); **52**, 287 (1985).
[7] J. E. White, *Underground Sound, Application of Seismic Waves* (Elsevier, New York, 1983).
[8] P. M. Morse and H. Feshbach, *Methods of Theoretical Physics* (McGraw-Hill, New York, 1953), pp. 882 and 1783.
[9] G. Arfken, *Mathematical Methods for Physicists,* 2nd ed. (Academic, New York, 1970).
[10] C. Kittel, *Introduction to Solid State Physics,* 6th ed. (Wiley, New York, 1986).
[11] L. I. Schiff, *Quantum Mechanics,* 3rd ed. (McGraw-Hill, New York, 1968), p. 283.
[12] G. D. Mahan, *Many-Particle Physics* (Plenum, New York, 1981).
[13] P. Sheng, in *Homogenization and Effective Moduli of Materials and Media,* edited by J. L. Ericksen, D. Kinderlehrer, R. Kohn, and J.-L. Lions (Springer-Verlag, Berlin, 1986).
[14] J. R. Beamish (private communication).
[15] E. Moly, P. Y. Wong, M. H. W. Chan, and J. R. Beamish, Phys. Rev. B **48**, 5741 (1993).